Research Article | Vol. 27, No. 26 / 23 December 2019 / Optics Express 38071
Optics EXPRESS

Integrated photonic tunable basic units using dual-drive directional couplers

DANIEL PÉREZ-LÓPEZ,* ANA M. GUTIERREZ, ERICA SÁNCHEZ, PROMETHEUS DASMAHAPATRA, AND JOSÉ CAPMANY

Photonics Research Labs, iTEAM Research Institute, Universitat Politècnica de València, Spain
*dperez@iteam.upv.es

Abstract: Photonic integrated circuits based on waveguide meshes and multibeam interferometers call for large-scale integration of Tunable Basic Units (TBUs) that feature beam splitters and waveguides. This units are loaded with phase actuators to provide complex linear processing functionalities based on optical interference and can be reconfigured dynamically. Here, we propose and experimentally demonstrate, to the best of our knowledge, for the first time, a thermally actuated Dual-Drive Directional Coupler (DD-DC) design integrated on a silicon nitride platform. It operates both as a standalone optical component providing arbitrary optical beam splitting and common phase as well as a low loss and potentially low footprint TBU. Finally, we report the experimental demonstration of the first integrated triangular waveguide mesh arrangement using DD-DC based TBUs and provide an extended analysis of its performance and scalability.

1. Introduction

Microelectronics has become one of the pillars of digital economics in the early 21st century. Current and emerging applications demand information processing at a faster speed and bandwidth, exposing a potential physical limitation of electronic systems. The cooperative use of electronics and photonics is being studied and applied as an appealing solution to overcome future performance limits, leveraging on the best of two worlds for both digital and analog processing.

Integrated photonics aims at the integration of a number of waveguide elements and specific devices or performance blocks to enable optical signal processing on a chip. Traditionally, both industry and academia have mainly focused on the design and optimization of Application Specific Photonic Integrated Circuits (ASPICs) whereby all the stages involved in the development of a PIC are tailored to optimize the chip performance, power budget, electrical power consumption, and footprint [1]. This strategy involves the optimization of photonic-based systems through multiple time-consuming cycles of custom design, fabrication, packaging and testing, leading to solutions that, in most cases, are far from being cost-effective for low and moderate volumes. Only very large volumes benefit from economies of scale, but as of yet, such applications are limited to data centre interconnects and transceivers [2].

Most of circuit designs for linear processing applications employ combinations of waveguide interconnections, beamsplitters, like directional couplers (DC), and phase actuators. The performance of each DC is highly dependent on its wavelength of operation, the waveguide geometry and the refractive indices of the materials [3]. These dependencies are in turn strongly influenced by nanometre scale geometrical fluctuations arising from factors such as fabrication deviations, variations in grown layer thickness, etc. which ultimately result in an equivalent shift of the wavelength of operation of such devices. On the other hand, reconfigurable phase shifters are circuit actuators that introduce a local phase shift of the optical signal when a control signal (typically electrical) is applied. These elements exploit different material properties to change the effective index of the waveguide: thermo-optic, electro-optic, magneto-optic, opto-mechanical, stress, etc. The integration of phase actuators is essential for the construction of operational

#379120 https://doi.org/10.1364/OE.27.038071
Journal © 2019 Received 30 Sep 2019; accepted 22 Nov 2019; published 16 Dec 2019

Optics EXPRESS

PICs, since their tunability can be employed to combat spurious effects arising from undesired geometric variations in the fabricated circuit. For example, a fixed optical filter can be tuned by adding extra phase shifters at key points in the optical circuit thus, compensating for the fabrication induced phase drifts [4].

In parallel, a paradigm shift in PIC design explores the development of multifunctional programmable circuits, where a common integrated optical hardware configuration is programmed to implement a variety of functionalities that can be elaborated for basic or complex operations in many application fields [5–8]. This approach enables a new generation of field-programmable PICs that will potentially offer cost-effective and ready-to-use solutions and allow upgradable photonic-based systems that provide post-compensation after a failure event [9]. Most of the experimental demonstrations reported to date use reconfigurable optical cores that comprise the interconnection of multiple unit cells known as Tunable Basic Units (TBUs) implemented by means of a tunable coupler in the form of 3-dB balanced dual-drive Mach-Zehnder interferometer with a phase shifter in each of its two arms [5–8]. However, to ensure the future scalability of these systems, research should be done in the optimization of these and other TBU architectures and tuning mechanisms with a view of reducing their insertion loss, footprint, optical crosstalk, and power consumption. In this paper, we propose the Dual-Drive Directional Coupler (DD-DC) as a candidate for the TBU implementation to achieve lower insertion losses and thus to increase the effective size of the circuits that can be programmed, [5]. In Section 2 we introduce the device configuration and operating principle. In Section 3 and 4 we present the experimental demonstration of a standalone component, in the context of conventional PIC layouts and as the key element in a waveguide mesh arrangement, respectively. Finally, in Section 5 we analyse the associated scalability issues and discuss their future evolution and applications.

2. Dual-drive directional couplers

The directional coupler is one of the most frequently employed basic building block in a PIC. Usually, it is designed to operate as a beam splitter characterised by a desired fixed optical power splitting ratio K at a certain wavelength. The signal in one waveguide is completely transferred to an adjacent, parallelly placed, waveguide at multiples of the so called coupling length L_c that depends on coupling constant κ, which in turn is a function of the wavelength of operation, the waveguide geometry and the refractive indices of the waveguide core and cladding materials [3]. These dependencies result in DCs being susceptible to fabrication errors that can change the designed wavelength of operation, bandwidth and uniformity.

The integration of a phase shifter in one of the arms of the coupler enables the tuning of the effective index difference between the two waveguides, and therefore the resulting coupling coefficient. This capability can be used to provide a tunable splitting ratio to the designed circuit as well as to compensate for fabrication variations. Standalone Tunable Directional Couplers (TDC) have been demonstrated in polymer materials [10–13], photonic crystals [14] and in Silicon on Insulator (SOI) [15], providing a reconfigurable splitting ratio by enabling a propagation constant difference in the pair of waveguides. The phase-change mechanisms are either based on a thermal-tuner placed on top of one of the parallel waveguides or on the use of the electro-optic effect to introduce a propagation constant difference between the waveguides. It should be pointed out that the setting of the coupling coefficient introduces an accumulated additional phase shift at each output of the coupler [15] which from an ideal standpoint is an undesired outcome.

In order to increase the capabilities of TDCs, the integration of a second phase shifter in the other waveguide can be considered with a view of providing a symmetric design in terms of the possible loss in each arm, as well as, and equally important, an independent setting of the beam splitting ratio and the additional phase shift through the induction of a differential and common phase shift, respectively, in each arm. This additional feature can find applications in

Optics EXPRESS

conventional PICs, but is particularly attractive for the implementation of compacts TBUs in waveguide mesh arrangements for programmable photonic circuits. A cross-section and top-view of a thermally tuned tunable dual-drive DC is illustrated in Fig. 1. The end-to-end analytical model is described in [9].

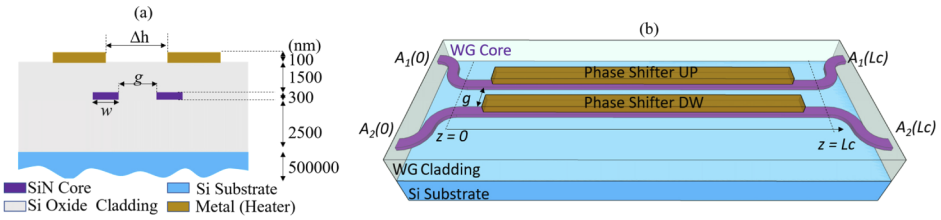

Fig. 1. Dual-Drive Directional Coupler (a) cross-section and (b) top-view.

3. DD-DC design and experimental demonstration

For the characterization of the DD-DC, we designed a chip layout based on a box-like waveguide cross section of 1 μm width (w) and 300nm height to satisfy the single-mode propagation condition. This geometry has been widely employed in previous Multi-Project Wafer (MPW) runs [16]. A mode solver was used, taking into consideration a central wavelength of 1.55 μm and the aforementioned geometric parameters, yielding a mode effective index of 1.5767, group index of 1.9234 and a second-order dispersion of -1.2027 ps/(nm·m) for the transverse electric (TE) fundamental mode.

The chip layout incorporates three layers: the optical waveguide, the metal layer and the thermal/optical isolation trench layer. The isolation layer involves etching up to the bottom-cladding layer, i.e. up to a depth of 1800 μm from the top cladding. The design incorporates DD-DCs as standalone elements and as tunable couplers in optical ring resonators (ORR) as well as the TBU in a triangular waveguide mesh arrangement consisting of five TBUs [5]. One key parameter in the configuration of a DD-DC is the phase difference between each of the two waveguides. As earlier noted, the propagation conditions are locally modified by a thermal-tuning effect produced by a microheater over the waveguide. The phase shift in a standalone waveguide is proportional to, [17]:

$$\Delta\phi = \Delta\beta \cdot L = \frac{2\pi}{\lambda}\Delta n_{eff} L = \frac{2\pi}{\lambda}\frac{dn_{eff}}{dT}\Delta T_{eff} \cdot L \tag{1}$$

where $\Delta\beta$ is the change in the propagation coefficient, L is the effective length of the phase actuator and Δn_{eff} is the change in the effective index, given by the multiplication of the thermo-optic coefficient (dn_{eff}/dT) and the effective temperature gradient (ΔT_{eff}) at the waveguide layer. Considering Eq (1), since the thermo-optic coefficient of silicon nitride is one order of magnitude lower than that of the SOI waveguide, a thermal actuator in silicon nitride requires a $\Delta T_{eff} \cdot L$ product, one order of magnitude greater than that in SOI to obtain the same phase shift. This effect translates into the need for considerably longer phase shifters.

Even considering that only one phase shifter is actuated, some tuning effects can exhibit a large spread as opposed to the effect being localised, which can lead to an induced and unwanted effective refractive index changes in the neighbouring waveguide. In the case of thermal actuators, the heat can flow to the adjacent waveguide and modify its propagation conditions. This effect can be modelled by using a thermal crosstalk coefficient (CT). Then, the difference between the phase alteration in an actuated waveguide with phase, $\Delta\Phi_1$, and a passive waveguide with phase,

Optics EXPRESS

$\Delta\Phi_2$, can be expressed as:

$$\Delta\phi_1 - \Delta\phi_2 = (\Delta\beta_1 - \Delta\beta_2)\cdot L = \frac{2\pi}{\lambda}L(\Delta n_{eff,1} - \Delta n_{eff,2}) = \frac{2\pi}{\lambda}\frac{dn_{eff}}{dT}L(\Delta T_{eff,1} - \Delta T_{eff,2}) = \frac{2\pi}{\lambda}\frac{dn_{eff}}{dT}L\cdot\Delta T_{eff,1}(1 - CT). \quad (2)$$

where, CT is in the range of 0 and 1. A DC design of this magnitude involves taking into account a trade-off between the device footprint and the minimum separation between the two arms of the DC. The latter is significant as it is limited by the technological limitation imposed by the fabrication of the photonic waveguide as well as the metallization forming the micro-heaters directly above said waveguides. Moreover, the proximity also determines the level of thermal crosstalk between adjacent arms. In this case, the proximity of the waveguides which was selected to maintain the footprint within a certain limit, means that the value of CT is very large. This thermal crosstalk coefficient can be estimated through simulations [17] or by comparing the efficiency of a dual-drive MZI and a DD-DC. Hence, in order to obtain a large phase difference between the waveguides, an even larger $\Delta T_{eff}\cdot L$ product is required. Increasing ΔT_{eff} is limited by the properties of the metal layer used to fabricate the micro-heaters over the waveguides. This comes from the fact that increasing the electrical power to the resistive heater-element can lead to an irreversible change in the material and even result in its melting [18]. In order to ensure that the phase shifters are long enough to be able to produce the required phase change, we designed passive cross-state configuration DD-DCs with a length of $L_{co} = 1278.73$ µm, and waveguide gap of 1.7 µm, as obtained from the passive mode-solver simulation displayed in Table 1. Some of the designs include variations of L_{co} to see which fabricated device yields the closest to the desired designed values.

Table 1. Simulated DC coupling length values for different gaps at wavelength of 1.55 µm

Gap (µm)	0.6	0.8	1.0	1.2	1.4	1.6	**1.7**
(w = 1 µm), L_{co} (µm)	58.2	101.7	180.6	311.2	543.7	945.4	**1278.73**
(w = 1.2 µm), L_{co} (µm)	90.6	163.6	301.2	565.0	1002.4	1852.3	TBD

In the following sections, we analyze the measured results for each DD-DC application.

3.1. Standalone DD-DCs

The first group of three components are TDC_1, TDC_2 and TDC_3. They are standalone DD-DCs with all ports accessible via edge-couplers. In order to investigate the translation of designed dimensions into the actual dimensions realised post-fabrication and to test the design tolerances, we have parameterized each coupler length to be: TDC_1: L_{co} = -30 µm, TDC2: $L_{co} = TDC_3$: L_{co} = +30 µm with all of them having separations of 1.7 µm between the two waveguides of a DC and 2.5 µm between micro-heaters. Using this combination of gap and coupling length, theoretically, we achieve a 1% uniformity in the coupling coefficient, across 18 nm.

Figure 2 shows the relevant section of the fabricated PIC and a labelled illustration of the mask layout. The upper (UP) and lower (DW) heaters and ports are labelled respectively.

In this design, we employed isolation trenches to focus the heat flow onto the waveguide and increase the actuator efficiency. Note that the isolation trenches are separated by more than 5 µm from the optical waveguides in order to prevent fabrication induced defects on the region close to the waveguide core and to avoid a mode interaction of the trench with the effective index. This safety distance was estimated to be around 3 µm by means of finding the negligible interaction distance between the mode and the trench through a mode-solver analysis.

Once fabricated, we characterized the components using both a conventional scheme involving a tunable laser and a synchronized optical spectrum analyser (OSA) as well as by means of a

Optics EXPRESS

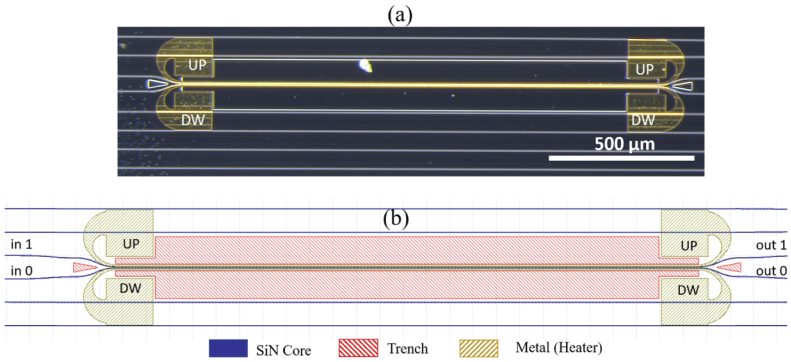

Fig. 2. Picture and labelled mask layout of standalone DD-TDC

broadband amplified spontaneous emission (ASE) light source. Using the tunable laser afforded us to measure higher extinctions with a greater precision but this came at the cost of a higher measurement time. The ASE source presents an instantaneous measurement but at the cost of a lower sensitivity which renders it incapable when measuring over a high dynamic range, for example when measuring large extinction ratios. The optical coupling was implemented using both lensed objectives and lensed fibers. In both schemes, we measured edge-coupling losses to be within a range of 3 dB/facet with a variability of ± 0.3dB. In regard to the electrical driving of the thermal actuators we probed the DC pads of each heater and employed a high precision Keithley current source. Unless specified, the measurements are single drive, i.e. only one heater is activated at a time.

In Fig. 3a, we illustrate the cross-port spectral response of TDC3, normalized with respect to the response of a 11mm long straight waveguide. We can see that a flat uniformity is maintained over the 6 nm range. Each trace corresponds to a different electrical driving condition where only one heater is employed. We can see that the power coupled to the opposite waveguide in a passive state (blue trace) is around 3 dB less than the maximum power (red trace), meaning that the targeted passive cross-state at the design stage is not achieved. If we set an electrical current in the upper phase shifter, we find a maximum of the total optical power in the cross-port (upper red-trace). If we drive the lower heater (DW), we find that the coupling ratio evolves in the opposite direction (i.e. decreases) till it reaches a minimum optical coupling at around -30dB (purple trace). A 0.2-dB ripple is observed in some of the measurements and is associated to the reflections in the measurement setup and the chip facets.

In order to characterize the dynamic behaviour of the structure, we performed continuous sweeps of electrical current with a step of 2 mA in one direction (upper heater) and then in the opposite (lower heater). For each case we measured the response for all input-output combinations. The cross-port power is directly proportional to the optical power coupling value (K) of the DD-DC. From the measurements illustrated in Fig. 3(b), it can be seen that the pattern is typical of a cross point interferometer and its complementary response as required by the conservation of energy during the configuration steps. We repeated the test for thirteen different TDCs in four different dies and five wafers and concluded that all the devices, except one displayed the same feature as in Fig. 3(b). When we tuned to the cross or bar states, we measured a portion of the signal that leaked over the non-desired output, (i.e. the optical crosstalk CT_{opt}). Overall, half of the measurements for the optical crosstalk in the cross and bar states were better than -15 dB. The measurement summary is displayed in Table 2. See Section 5.2 for additional details and for a performance comparison with a Dual-Drive MZI.

From the measurements, we can see that some of the DD-DC showed a non-ideal behaviour with CT_{opt} over -15 dB in either cross or bar. This behaviour was present in more than 50% of

Optics EXPRESS

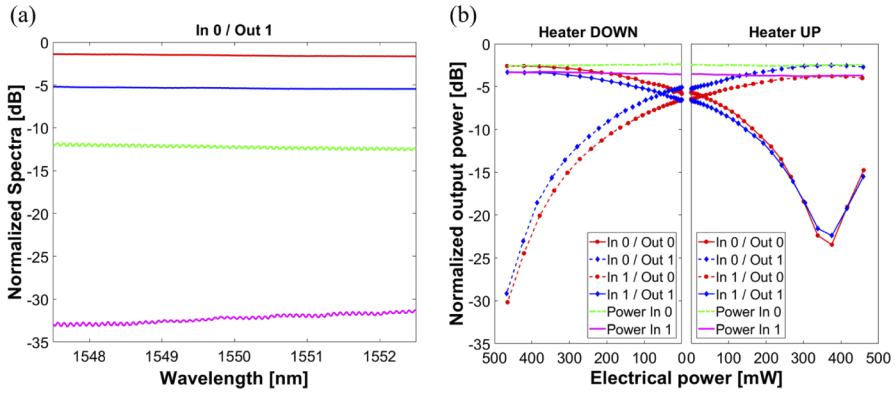

Fig. 3. (a) Spectral response of the DD-TDC 3 and (b) Experimental spectral response of a DD-TDC when upper or lower phase shifters are actuated.

Table 2. Measurements of standalone DD-DC summary (CT: Optical Crosstalk, Pe: Electrical Power)

item	Wafer	Die	TDC#	CT bar (dB)	CT cross (dB)	Pe bar (mW)	Pe cross (mW)
1	1	5	1	12.732	14.184	431.92	317.35
2	1	6	3	15.339	14.509	455.42	284.12
3	2	3	3	29.034	11.534	399.12	445.65
4	3	4	3	16.588	11.993	528.70	165.57
5	3	5	1	4.216	17.937	429.97	162.45
6	3	5	2	12.790	16.626	453.17	242.75
7	3	5	3	25.698	16.196	454.90	346.85
8	4	4	2	6.193	13.982	465.85	100.28
9	4	4	3	10.647	22.509	316.97	489.17
10	4	5	1	16.557	19.834	440.22	295.85
11	4	5	2	26.704	19.775	466.47	375.27
12	4	5	3	28.600	19.828	380.60	429.20
13	5	4	3	25.313	16.398	524.87	278.77

the measured TDCs, independently of the coupling length. These results are a consequence of the low fabrication tolerance of the DCs. In addition, all the CT_{bar}(dB) could be improved by not limiting the maximum applicable current to 40 mA. However, there was a high-risk of achieving a breaking point when driving the heater with larger electrical currents.

Due to the facet and alignment variation, it is challenging to estimate the insertion loss of the DD-DC. To do so, we measured an additional set of 26 samples of which the 76.92% showed an insertion loss below 0.2 dB. Finally, by computing the sum of the optical power in both outputs, we saw that the conservation of energy was maintained during the dynamic configuration of every sample.

3.2. DD-DC in photonic integrated circuits

The DD-DC can be integrated in a wide variety of PICs requiring both, an arbitrary beam-splitting and a phase adjustment. For example, its integration in an optical ring resonator enables the independent modification of the notch position and the extinction ratio.

Optics EXPRESS

In these designs, we have employed the same waveguide separation of 1.7 μm, distance between heaters of 2.5 μm and a coupling length of $L_{co} + \Delta L$ with length variations (ΔL) equal to: -100, -50, 0, 50 μm. These values have been chosen in order to account for the coupling length variation with changes in the waveguide geometry. For these lengths we created a replica with a larger distance between heaters of 3μm, resulting in a total of 8 optical ring resonators. Coupling length has been estimated to vary by ± 100 μm for waveguides with width variations of ± 20 nm. Figure 4(a) and (b) show the zoomed image of the fabricated device and the designed mask layout respectively.

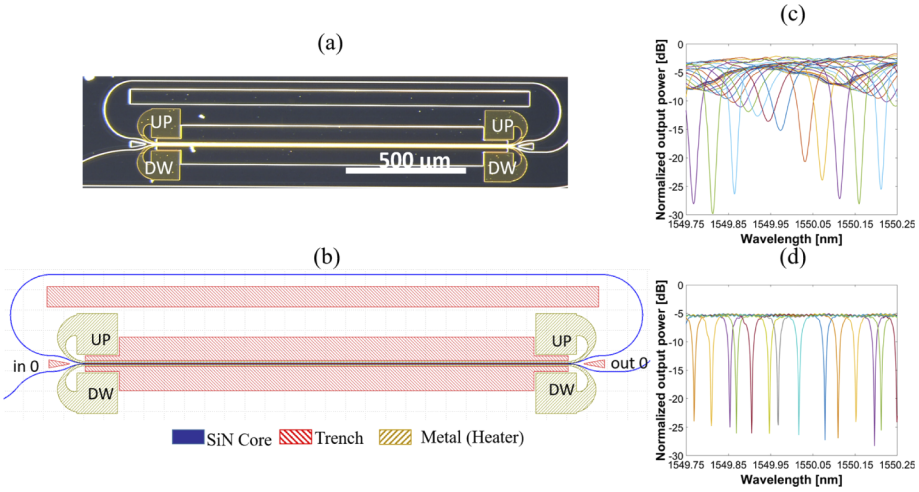

Fig. 4. (a) Zoomed image (b) labelled mask layout: Ring-loaded version of DD-TDC for its characterization and (c) example of resulting spectral response with single-drive operation with each trace referring to a progressively increasing electrical power driving in one of the heaters, (d) example of notch wavelength tuning with dual-drive operation with each trace referring to a progressively increasing electrical power driving both heaters, simultaneously.

When modifying the coupling coefficient by actuating one of the phase tuners (UP or DW), we produce a power splitting ratio variation as illustrated in Fig. 3(b). This can be employed to modify the extinction ratio of the optical filter as shown in Fig. 4(c). Each trace refers to a progressively increasing electrical power driving in one of the heaters. However, as illustrated in the figure, these changes introduce a common phase shift at the DD-DC outputs, moving the position of the notch as well. If the splitter is integrated in a large-scale circuit, we might want to correct this accumulated phase and set the coupling factor and the accumulated phase independently. Figure 4(d) illustrates how a dual-drive operation can be employed to maintain the ER over 19 dB while effectively tuning the wavelength position of the notch by driving the DC in dual-drive mode. Each trace refers to a progressively increasing electrical power driving both heaters, simultaneously.

To obtain a better understanding of the dual-drive behaviour, Fig. 5 represents in a contour plot, the experimental results of the ER and phase shift tuning of a ring resonator with a tunable coupler based on DD-DCs. Here, we mapped the extinction ratio (ER) and the phase shift versus the electrical power applied to both heaters simultaneously. We can obtain two conclusions from Fig. 5(a). First, we see that any arbitrary ER of the ring can be set from 0 to at least, 24 dB by optimally tuning the electrical power of one heater, exclusively. Secondly, it can be seen that there is a plane where the ER is almost constant once the targeted ER is set and an additional common-drive is applied simultaneously to both heaters. From Fig. 5(b), we can extract two complementary conclusions. First, it is confirmed that a single-drive configuration will modify

Optics EXPRESS

both the ER and the phase shift (notch position). Secondly, the application of the aforementioned common drive is translated to a linear variation of the overall phase shift (notch position, only).

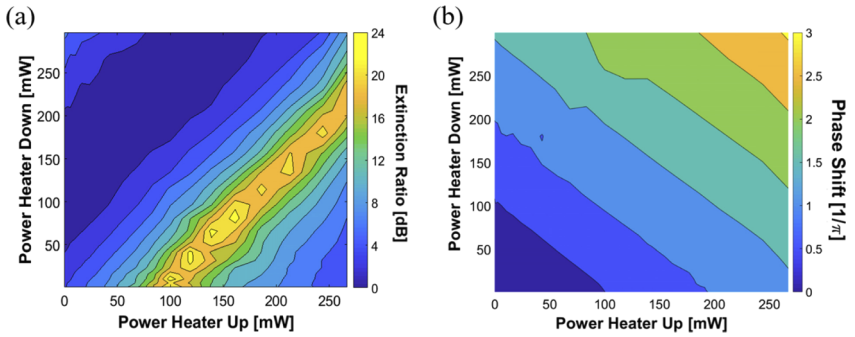

Fig. 5. (a) Extinction Ratio and (b) phase shift variation of a single-notch ORR with a DD-DC (1328.73 µm).

Experiments, as a whole, determine that once fixed to a targeted ER by driving one of the phase shifters, we can drive both heaters with an additional common power in both actuators to set the notch position without seriously compromising the set ER value. Note that the phase change should be linear with the applied electrical power. In that case, we would expect a common drive to imply the same power being applied to both after the initial condition is reached. However, in the common-mode, a light discrepancy between the required electrical powers per heater can be extracted from the measurements, due to proximity and thermal crosstalk effects.

For these measurements, we employed a tunable laser and a synchronized OSA with the system having a 1 pm resolution. We measured 10 structures obtaining similar trends and behaviours.

Additionally, we have explored the effects of including a thermal isolation in the form of an air trench between the two adjacent waveguides. For this purpose, we designed an additional set of ORRs with length variations of: 1000, 1200, 1400 and 1600 µm. Figure 6 illustrates the experimental results obtained in a DD-DC with a coupling length of 1200 µm. From the results, we see that this time the ER maximum value is higher, but we did not apply enough electrical power to the heaters, in order to achieve the bar state that can be characterized by a 0-dB ER value. This was done to prevent the said heaters from achieving a non-reversible melting state. In addition, the ER is also limited by the reflections at the facets of the chip couplers.

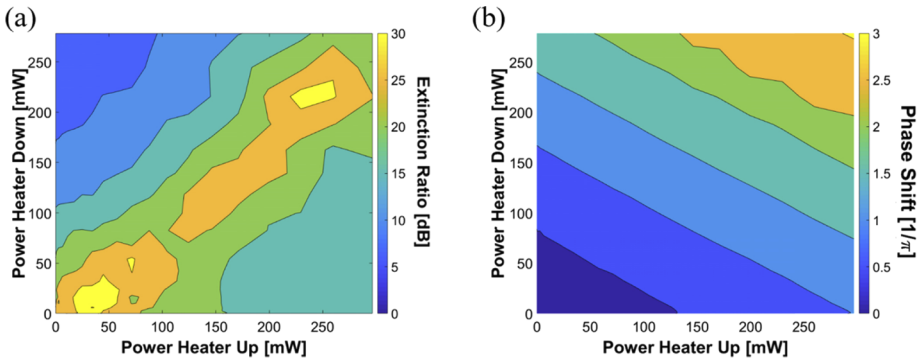

Fig. 6. (a) Extinction ratio and (b) phase shift variation of a single-notch ORR with a DD-DC (1200 µm) and with an isolation trench between the waveguides.

Optics EXPRESS

However, as in the previous section, we found some randomness in the measured performance of both DD-DC designs that might be again related to the fabrication tolerances of the device and noise during the measurements.

4. DD-DCs based tunable basic units for waveguide mesh arrangements

A novel class of programmable photonic ICs employs a massive interconnection of beamsplitters and phase shifters to produce multiport interferometric patterns. These arrangements have been proposed based on the replication of TBUs and their interconnection either in a feedforward topology [6] or by allowing light recirculation and feedback loops [5,7-9]. Most of the demonstrations rely on TBUs based on thermally actuated Mach-Zehnder interferometers loaded with one phase shifter on each arm. The performance and versatility of these circuits are limited by the number of integrated TBUs. The scalability of this approach is constrained by the excess loss of each TBU, the optical crosstalk, the power consumption and the footprint. The losses being one of the main limitations, a waveguide mesh circuit becomes impractical when employing TBUs with moderate insertion losses (> 0.4 dB) [9] and with optical crosstalk below 20 dB [18]. Due to the significant number of TBUs that need to be traversed by the signal in a circuit in order to enable a certain degree of interconnection complexity, a minimal improvement in the TBU insertion loss has a remarkable impact on the overall mesh design and performance. To achieve this, we analyze the possibility of implementing the TBUs using the designed DD-DC instead of a 3-dB MZI. A 3-dB MZI employs two optical couplers to split and combine the light so with this approach, an arbitrary waveguide mesh arrangement would require half of the number of optical couplers, reducing the overall insertion loss of the programmed circuits. However, additional performance metrics like optical crosstalk, fabrication tolerance, footprint, and power consumption should be analysed accordingly.

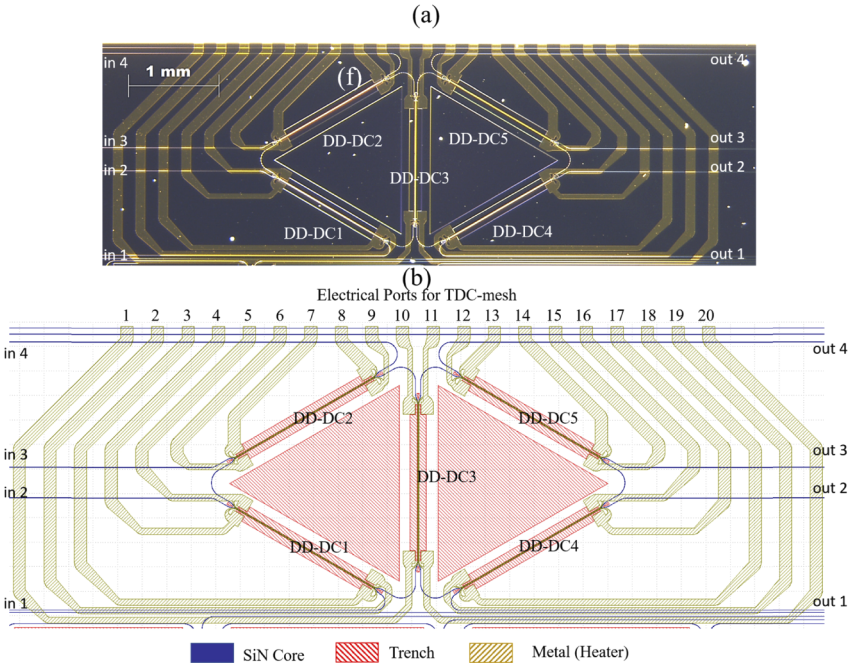

Fig. 7. (a) Chip image and (b) labelled mask layout of a triangular waveguide mesh based on DD-DC tunable elements.

Optics EXPRESS

Figure 7 shows the first implementation of a triangular waveguide mesh arrangement and the first waveguide mesh arrangement exclusively based on DD-DCs. It is composed of 5 TBUs (with 5 optical couplers), building-up two triangular cells, 8 optical ports and 10 phase shifters.

In this simple structure we can program each TBU to be implemented either as a photonic switch (by setting the TBU to cross or bar) or as a beam splitter, providing any arbitrary splitting ratio. In addition, a common phase term can be locally added to the outputs of each TBU, as we demonstrated in the previous section. With all these functions, one can discretize conventional PICs into TBU primitives. First, we characterized all the TBU responses by using the mesh characterization protocol recently proposed [19]. Afterwards, we were able to program different structures like delay lines, a single ring resonator, an add-drop filter (transmission and reflection response), and a coupled resonant waveguide (CROW) made of two cavities.

Figure 8(a1) describes the single ring resonator implementation. Here, TBU_1 is configured as a tunable coupler, TBU_2 and TBU_3 are configured as switches in their bar state. The reflection response is obtained employing input port 1 and output port 2 as illustrated in Fig. 8(bc1). Furthermore, as illustrated in Fig. 8(b1), we can now exploit the independent phase shifting capabilities of DD-DCs and tune the position of the notch over the full Free Spectral Range without seriously compromising the extinction ratio. Each trace refers to a different electrical driving setting, ranging between 0 and 20 mA (up to around 60 mW). Next, we reprogrammed the mesh to perform an add-drop filter by modifying the TBU_3 configuration to an arbitrary tunable coupler configuration, as shown in Fig. 8(a1). We then measured the reflection and transmission (Fig. 8(c1)) responses of the ring. Note that we have optimized them separately. The extinction ratios are 24 and 17 dB in the reflection and transmission response, respectively.

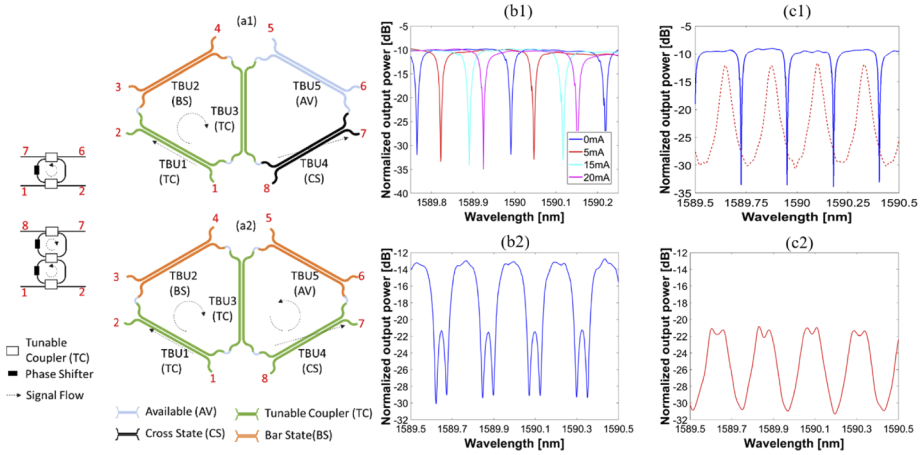

Fig. 8. Triangular feedforward/feed-backward waveguide mesh arrangement based on DD-DC units. For a single ring resonator and add-drop: (a1) Targeted layout and TBU settings, (b1) Reflection response of the single ring resonator for different electrical driving configurations ranging between 0 and 20 mA (up around 60 mW) per heater and (c1) Transmission (dotted) and reflection (solid) responses for an add-drop configuration. For a coupled ring resonator structure: (a2) Targeted layout and TBU settings, (b2) Reflection and (c2) Transmission responses.

The next example illustrates the synthesis of two coupled optical cavities. Again, we employ the input port 1. The reflection response is obtained from output port 2 (Fig. 8(b2)) and the transmission response from output port 7 (Fig. 8(c2)). In this case, the measured ER was 8 and 9 dB, respectively.

Optics EXPRESS

5. Discussion

5.1. Theoretical background

The experimental work reported in this paper validates the behaviour of the DD-DC as a 2×2 optical component that enables independent setting of a tunable splitting ratio and a common phase shift at its outputs. We have however measured an unexpected non-symmetrical behaviour between the actuation of the phase shifters. Going deeper into the theoretical framework, directional couplers have been modelled by using coupled-mode equations. These analyses on passive designs have been extended to account for single-drive and for differential modulation schemes and the possibility of altering the propagation conditions of each arm in a differential way [3] or independently [9]. According to these, we would have expected that both phase actuators should provide a symmetric effect when tuning any of the phase shifters in a single-drive mode. However, the proposed theoretical solutions assume that the coupling factor between waveguides (κ) remains constant during the tuning and symmetrical (the coupling factor from waveguide 1 to waveguide 2 is equal to the coupling factor from waveguide 2 to waveguide 1). Under these conditions, independently of the phase actuator employed (upper or lower) in a DD-DC, the overall splitting ratio would tend to κ equal to zero first and small oscillations would appear around the bar operation point, decoupling the waveguide interaction.

However, the propagation coefficient modification of each waveguide has a direct impact on the coupling factor between the two waveguides (κ_{10}, κ_{01}) [20], which is behind the non-even function dependency for each phase actuator. In addition, it should be expected that the tuning effect will modify the refractive index of the cladding with a different proportion for each waveguide. This is the reason behind the asymmetrical / non-even behaviour of the DD-DC reported in this paper.

5.2. Comparison between dual-drive directional coupler and dual-drive mach Zehnder interferometer

Any TBU of a mesh-based programmable photonic IC should provide full flexibility in the configuration of both amplitude and phase, while offering low insertion loss, low power consumption, low optical crosstalk, and low footprint. In this way, both Directional Couplers and Mach Zehnder Interferometers can incorporate phase tuning elements in both arms to achieve the basic operation [5, 6, 7]. Obtaining good-enough metrics in the mentioned key performance indicators is essential to ensure the scalability of large-scale programmable photonic circuits in general and of optical meshes, in particular.

Firstly, optimizing the TBU by minimizing the IL per basic optical delay ratio is crucial to achieve higher performance as well as to reduce the total footprint of the circuit. Secondly, the reduction of the power consumption of a TBU have a massive impact in the overall power consumption of the circuit. Finally, reduced insertion losses are key to preserve the signal quality at the end of the mesh. Eventually, although purely SOI and Si_3N_4 have been employed for the development of phase actuators for programmable devices, other platforms as polymer [13] and other or materials integrated on silicon, such as graphene [23] or transition metal oxides [24,25] have been also proposed, which appears as exciting research route for the optimization of the metrics needed for the future programmable photonic ICs.

Almost all the waveguide-mesh implementations proposed so far rely on TBUs implemented by means of MZIs with two 3-dB couplers. This TBU design offers a wideband tunable operation, but the scalability of the circuit is mainly limited by the insertion loss (IL) resulting from the required pair of 3 dB splitters. This accumulated IL, results in an even higher loss across the circuit as it accumulates depending on the number of TBUs traversed. In this way, the DC is presented as the perfect contender to overcome such limitations. Although the thermo-optic effect is presented as a proof-of-concept and might be substituted by alternative phase mechanisms, the position and geometry of the heaters and the DC cross section could be optimized to increase

Optics EXPRESS

the efficiency of the presented solution, while reducing both footprint and the total optical delay. However, the optimization of the thermally tuned DD-DC is constrained by fabrication limitations that set minimum distances between metal layers and waveguide layers, among waveguide layers and safety distances for isolation trenches.

For comparison purposes between the two structures, the following table covers the performance of MZIs and DD-DCs reported in the literature. Although the number of reported MZIs is extensive, we selected the ones that have been employed as TBU in waveguide mesh arrangements or optical switching networks.

As it can be extracted from Table 3, the MZI employed for the 32×32 switch in silicon on insulator in [26] presented very low power consumption but high losses per switch unit. The losses are mainly related to the 3-dB couplers and the additional loss imposed by the tuning mechanism. Also in SOI, a similar power consumption and length but greater insertion loss as compared with our DD-DC were shown for the MZI switch unit in [27]. Comparing with one of our previous works [8], a MZI with lower size and power consumption was experimentally demonstrated in silicon on insulator, but again, the insertion losses were higher than the one presented in our current design, due to the two-fold 0.2-dB per multimode interferometer at the MZI. The DD-DC that we presented in [9] consist of a first design iteration, with a similar length. It was estimated to offer low losses of 0.1dB but required a power consumption 110-mW higher than the current one. Orlandi et al. presented in [15] a very compact DC with a very low power consumption but with no dual-drive configuration, and therefore with no phase-control capability. Although a full-coupling tuning was not achieved in the work, it can be inferred that a DD-DC in silicon on insulator can be designed with a lower footprint and with low insertion loss.

Table 3. Comparison between DC and MZI devices (P_{π} : Electrical power required to tune the couplers from 0 to 100% coupling, (B): Bar, (C): Cross, SD: Single Drive, EO: Electro-optic, TO: Thermo-optic)

Ref.	Device	Technology	Effect	Length (μm)	Insertion Losses (dB)	P_{π}. (mW)
[26]	MZI	Si	EO	334[a]	1.5 (B) & 1.3 (C)[b]	3.76(B) & 1.71 (C)[c]
[27]	MZI	Si_3N_4	TO	1173[d]	0.61 (B) & 1.17 (C)[e]	360
[8]	MZI	Si	TO	975	0.6dB ± 0.1dB	110 ± 15
[7]	MZI	Si_3N_4	TO	2450	not reported	350
[9]	DD-DC	Si_3N_4	TO	1235	0.1[f]	460
[15]	SD-DC	Si	TO	74	not reported	36
OUR	DD-DC	Si_3N_4	TO	1278.73	0.2dB	350

[a]Calculated using a 200 μm length PIN phase shifter and 68.5 μm length MMI as obtained from [26]
[b]Calculated considering the switch unit and access waveguide and excluding the crossings
[c]The total power consumptions of the 32×32 switch was 542.3(B) & 247.4 (C) and integrates 144 units.
[d]Calculated using L_{MMI}=46 μm, $L_{input/ouput\_WG\_MMI}$=8 μm, $L_{electrode}$=750 μm; Angle = 90° and R = 100 μm as obtained from [27]
[e]Calculated using 3.08 dB excess loss for 5MZIs path (bar) 4.71 dB excess loss for 4 MZI path (Cross) as obtained from [27]
[f]Rough estimation due to alignment and facets variability [9].

All in all, it the use of a DD-DC seems a potential solution, both in silicon and silicon nitride, to overcome the scalability limitations of programmable photonic integrated circuits related to the insertion loss, while maintaining a comparable length to the MZI approach. Power consumption is compromised and future research is required either in the optimization of thermo-optic based architectures or in the search of alternative methods.

Optics EXPRESS

5.3. Large-scale programmable circuits

The versatility and performance of mesh-based optics is proportional to the number of integrated TBU. However, in practice, several issues like footprint and space requirements, as well as electrical interfacing and electrical routing limit their scalability. These problems are common for meshes composed of both DD-DC and MZIs. We briefly analyze the most important ones below [28].

Footprint: The footprint of the mesh is a function of the area of the Tunable Basic Unit and the number TBUs. In order to reduce this footprint, platforms that provide a higher refractive index contrast and thus smaller waveguides, such as SOI [29] or Si_3N_4 are used. In contrast, higher integration density becomes an issue if the thermo-optic effect is employed as the tuning mechanism due to the thermal crosstalk between the neighboring units, [35]. This set a trade-off between footprint and thermal crosstalk which needs to be taken into account in order to achieve the most optimal design.

Electrical routing: The use of large-scale mesh arrangement turns into a challenge when considering the routing of all the metal tracks of each reconfigurable component and a small targeted circuit footprint. As we increase the size of the programmable optical core, we need a more complex scheme of layers to carry out the routing. As an example, Table 4 illustrates how the number of MZIs, bond pads, thermal tuners and optical inputs/outputs raise when a waveguide mesh arrangement of a linear multiport interferometer is scaled [19]. This increment in complexity would equally affect a design employing DC-DD, since they would have the same number of bond pads and thermal tuners as the MZIs.

Table 4. Comparative table between the number of cells and the number of devices needed

Cells Number	MZIs	Thermal Tuners	Pads	Optical I/O
8	35	70	140	28
7	30	60	120	24
6	27	54	108	24
5	24	58	116	24
4	19	38	76	20

In practice, the number of electrical tracks and its associated control system becomes a serious limit for the number of TBUs that can be present in the circuit. One solution consists of sharing the ground pad in the circuit, which can then reduce the number of electrical tracks and pads by a factor of almost two. The main drawback would be then the appearance of electrical crosstalk, which can be pre-characterized seeing the differential resistance of each path [30], or mitigated by using electrical current sources.

Electrical interfacing: Along the same lines, the elements inside the programmable photonic processor are driven by electrical signals coming from electrical circuits that can be or not integrated. The interface between the electrical pads and the electrical circuits can be done using wire-bonding techniques to connect the electrical channels of the PIC to a printed circuit board (PCB). However, this require a certain minimum pitch between bond pads in the PIC (typically 100-150 µm) to avoid crossings between wires as well as a minimum bond pad size (usually in the order of 60-100 µm), imposing a limit in the number of electrical channels [19]. To overcome this limit, more bond pads can be integrated if the electrical interfacing is done flip-chip techniques [31].

Although the number of tunable units and its electrical interfacing is a current research challenge, a large number of optical switching matrix has been demonstrated very recently. Although the functionality and requirements are fundamentally different from the waveguide mesh arrangements covered in this paper, some of the specifications and system integration

Optics EXPRESS

challenges are common. In the optical switching field, the community has been focused on the development of large-scale switch matrices and their integration with electronics. An example, a 32-port MZI-based silicon electro-optical switch has been reported integrated in silicon on insulator and interfaced with wire bonding schemes using 450 thermally tuned TBUs [32,33]. A 64×64 photonic MEMS-actuated adiabatic coupler switch with 4096 switching cells and low on-chip loss has been also demonstrated by researchers at California-Berkeley University [34].

All in all, the proposed architecture can find applications in any PIC requiring reconfigurable beamsplitting and phase shifting. Figure 9 illustrates examples of their local application in coupled-ring structures, MZIs and waveguide meshes. According to the latter, the proposed architecture reduces the insertion loss of Tunable Basic Units, allowing an increment in their scalability and versatility. However, future development requires the optimization of the device to increase its tolerance to fabrication variations to maintain an optical crosstalk better than 20 dB in the targeted wavelength range. With regard to power consumption, the thermo-optic effect requires around 350 mW to tune to either bar or cross state. The high-power requirement arises from the waveguidés low thermo-optic coefficient and the high thermal crosstalk coefficient in between them. To ensure the future evolution of DD-DC, it should be integrated on a SOI platform or alternative tuning mechanisms should be explored. The current demonstration is the seed for future works that will potentially combine the proposed architecture with, for example, a non-volatile phase change material [21,22], maintaining the decrement in insertion losses and allowing near-zero power consumption. Finally, the footprint of the device is highly influenced by the length required for the desired tuning and should be in the range of hundreds of micrometres to allow high-density integration.

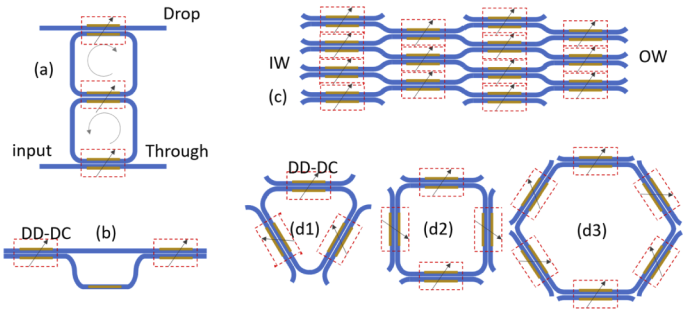

Fig. 9. Photonic integrated circuits with Dual-Drive Directional Couplers. (a) add-drop, (b) Mach-Zehnder Interferometer, (c) arbitrary unitary linear multiport interferometer, (d) feedback-enabled waveguide meshes IW: input waveguides, OW: output waveguides.

6. Conclusions

The very-large integration density required in future field-programmable photonic integrated circuits and waveguide meshes calls for the optimization of their Tunable Basic Units. Here, we have proposed a new component based on adding two extra phase actuators to the conventional directional coupler. Leveraging on the thermo-optic effect, we have experimentally demonstrated that it is possible to set, independently, the coupling ratio and an overall phase increment that can find applications in programming conventional photonic integrated circuits and in waveguide mesh arrangements. The latter are proposed as a possible option to overcome insertion losses and reduce internal reflections. Future work is required to increase the fabrication tolerances and improve the power consumption.

Optics EXPRESS

Funding

European Research Council (ERC ADG-2016 UMWP-Chip, ERC-POC-2019 FPPAs); Generalitat Valenciana (PROMETEO 2017/017); European Cooperation in Science and Technology (COST Action CA16220 EUIMWP.).

Disclosures

The authors declare no conflicts of interest.

References

1. R. Soref, "The Past, Present and Future of Silicon Photonics," IEEE J. Sel. Top. Quantum Electron. **12**(6), 1678–1687 (2006).
2. D. Inniss and R. Rubenstein, "*Silicon photonics, Fuelling the Next Information Revolution*," (Morgan Kaufmann, 2016).
3. S. Somekh, E. Garmire, A. Yariv, H. L. Garvin, and R. G. Hunsperger, "Channel Optical Waveguides and Directional Couplers in GaAs–Imbedded and Ridged," Appl. Opt. **13**(2), 327–330 (1974).
4. C. K. Madsen and J. H. Zhao, "*Optical Filter Design and Analysis: A Signal Processing Approach*," (Wiley, 1999).
5. D. Pérez, I. Gasulla, J. Capmany, and R. Soref, "Reconfigurable lattice mesh designs for programmable photonic processors," Opt. Express **24**(11), 12093–12106 (2016).
6. W. R. Clements, P. C. Humphreys, B. J. Metcalf, W. S. Kolthammer, and I. A. Walmsley, "Optimal design for universal multiport interferometers," Optica **3**(12), 1460–1465 (2016).
7. L. Zhuang, C. G. H. Roeloffzen, M. Hoekman, K.-J. Boller, and A. J. Lowery, "Programmable photonic signal processor chip for radiofrequency applications," Optica **2**(10), 854–859 (2015).
8. D. Pérez, I. Gasulla, L. Crudgington, D. J. Thomson, A. Z. Khokhar, K. Li, W. Cao, G. Z. Mashanovich, and J. Capmany, "Multipurpose silicon photonics signal processor core," Nat. Commun. **8**(1), 636 (2017).
9. D. Pérez, E. Sánchez, and J. Capmany, "Programmable True-Time Delay Lines using integrated waveguide meshes," J. Lightwave Technol. **36**(19), 4591–4601 (2018).
10. H. Kogelnik and R. V. Schmidt, "Switched directional couplers with alternating $\Delta\beta$," J," Quantum Electron. **12**(7), 396–401 (1976).
11. R. V. Schmidt and H. Kogelnik, "Electrooptically switched coupler with stepped $\Delta\beta$ reversal using Ti-diffused $LiNbO_3$ waveguides," Appl. Phys. Lett. **28**(9), 503–506 (1976).
12. R. C. Alferness and J. J. Veselka, "Simultaneous modulation and wavelength multiplexing with a tunable Ti: $LiNbO_3$ directional coupler filter," Electron. Lett. **21**(11), 466–467 (1985).
13. A. Sahmah and M. Supa'at, "Implementation of thermo-optic waveguide photonics switch using polymer material," in *Proceedings of IEEE 4th International Conference on Photonics (ICP2013)*, pp. 33–37.
14. A. Sharkawy, S. Shi, D. W. Prather, and R. Soref, "Electro-optical switching using coupled photonic crystal waveguides," Opt. Express **10**(20), 1048–1059 (2002).
15. P. Orlandi, F. Morichetti, M. J. Strain, M. Sorel, A. Melloni, and P. Bassi, "Tunable silicon photonics directional coupler driven by a transverse temperature gradient," Opt. Lett. **38**(6), 863–865 (2013).
16. G. Micó, L. A. Bru, D. Pastor, D. Doménech, J. Fernández, A. Sánchez, J. M. Cirera, C. Domínguez, and P. Muñoz, "Silicon nitride photonics: from visible to mid-infrared wavelengths," Proc. SPIE **10537**, 105370B (2018).
17. D. Pérez, J. Fernández, R. Baños, J. D. Doménech, A. M. Sánchez, J. M. Cirera, R. Mas, J. Sánchez, S. Durán, E. Pardo, C. Domínguez, D. Pastor, J. Capmany, and P. Muñoz, "Thermal tuners on a Silicon Nitride platform," https://arxiv.org/abs/1604.02958.
18. D. Pérez and J. Capmany, "Scalable analysis for arbitrary photonic integrated waveguide meshes," Optica **6**(1), 19–27 (2019).
19. D. Pérez, "Integrated microwave photonic processors using waveguide mesh cores", Ph.D. Thesis, 2017.
20. B. E. Saleh and M. C. Teich, "*Fundamentals of photonics*," (John Wiley & Sons, 2019).
21. C. Rios, M. Stegmaier, Z. Cheng, N. Youngblood, C. D. Wright, W. H. P. Pernice, and H. Bhaskaran, "Controlled switching of phase-change materials by evanescent-field coupling in integrated photonics [Invited]," Opt. Mater. Express **8**(9), 2455–2470 (2018).
22. J. Zheng, A. Khanolkar, P. Xu, S. Colburn, S. Deshmukh, J. Myers, J. Frantz, E. Pop, J. Hendrickson, J. Doylend, N. Boechler, and A. Majumdar, "GST-on-silicon hybrid nanophotonic integrated circuits: a non-volatile quasi-continuously reprogrammable platform," Opt. Mater. Express **8**(6), 1551–1561 (2018).
23. J. Capmany, D. Domenech, and P. Muñoz, "Silicon graphene waveguide tunable broadband microwave photonics phase shifter," Opt. Express **22**(7), 8094–8100 (2014).
24. S. Abel, F. Eltes, J. E. Ortmann, A. Messner, P. Castera, T. Wagner, D. Urbonas, A. Rosa, A. M. Gutierrez, D. Tulli, P. Ma, B. Baeuerle, A. Josten, W. Heni, D. Caimi, L. Czornomaz, A. A. Demkov, J. Leuthold, P. Sanchis, and J. Fompeyrine, "Large Pockels effect in micro- and nanostructured barium titanate integrated on silicon," Nat. Mater. **18**(1), 42–47 (2019).

Optics EXPRESS

25. L. Sanchez, S. Lechago, A. M. Gutierrez, and P. Sanchis, "Analysis and Design Optimization of a Hybrid VO_2/Silicon 2 (2 Microring Switch," IEEE Photonics J. **8**(2), 1–9 (2016).
26. L. Qiao, W. Tang, and T. Chu, "32×32 silicon electro-optic switch with built-in monitors and balanced-status units," Sci. Rep. **7**(1), 42306 (2017).
27. D. Zheng, J. D. Doménech, W. Pan, X. Zou, L. Yan, and D. Pérez, "Low-loss broadband 5×5 non-blocking Si_3N_4 optical switch matrix," Opt. Lett. **44**(11), 2629–2632 (2019).
28. D. Pérez, I. Gasulla, and J. Capmany, "Programmable Multifunctional Photonics ICs," in *IEEE Proceedings of Photonics in Switching and Computing (PSC2018)*
29. J. Capmany, I. Gasulla, and D. Perez, "Microwave photonics: the programmable processor," Nat. Photonics **10**(1), 6–8 (2016).
30. J. Carolan, C. Harrold, C. Sparrow, E. Martín-López, N. J. Russell, J. W. Silverstone, P. J. Shadbolt, N. Matsuda, M. Oguma, M. Itoh, G. D. Marshall, M. G. Thompson, J. C. F. Matthews, T. Hashimoto, J. L. O'Brien, and A. Laing, "Universal linear optics," Science **349**(6249), 711–716 (2015).
31. J. Muller, M. Noren, M. Mach, S. Brunner, and C. Hoffmann, "Small size LTCC FlipChip-package for RF-power applications," in *IEEE Proceedings of European Microelectronics and Packaging Conference (EMPC2009)*, pp. 1–4.
32. D. Celo, D. J. Goodwill, J. Jiang, P. Dumais, C. Zhang, F. Zhao, X. Tu, C. Zhang, S. Yan, J. He, M. Li, W. Liu, Y. Wei, D. Geng, H. Mehrvar, and E. Bernier, "32 × 32 silicon photonics switch," in *IEEE Proceedings of 21st OptoElectronics and Communications Conference (OECC2016)*, WF1-4.
33. B. G. Lee and N. Dupuis, "Silicon photonic switch fabrics: technology and architecture," J. Lightwave Technol. **37**(1), 6–20 (2019).
34. T. J. Seok, N. Quack, S. Han, R. S. Muller, and M. C. Wu, "Large-scale broadband digital silicon photonic switches with vertical adiabatic couplers," Optica **3**(1), 64–70 (2016).
35. M. Milanizadeh, S. Ahmadi, D. Aguiar, A. Melloni, and F. Morichetti,. "Efficient thermal cross-talk effect cancelation in photonic integrated circuits," *2019 Optical Fiber Communications Conference and Exhibition (OFC)*, 1–3, (2019).